

xView3-SAR: Detecting Dark Fishing Activity Using Synthetic Aperture Radar Imagery

Fernando S. Paolo^{2,*}, Tsu-ting Tim Lin^{3,*}, Ritwik Gupta^{1,4,*†}, Bryce Goodman¹, Nirav Patel¹, Daniel Kuster³, David Kroodsma², Jared Dunnmon¹

¹Defense Innovation Unit, ²Global Fishing Watch, ³Cambrío, ⁴UC Berkeley

Abstract

Unsustainable fishing practices worldwide pose a major threat to marine resources and ecosystems. Identifying vessels that evade monitoring systems—known as “dark vessels”—is key to managing and securing the health of marine environments. With the rise of satellite-based synthetic aperture radar (SAR) imaging and modern machine learning (ML), it is now possible to automate detection of dark vessels day or night, under all-weather conditions. SAR images, however, require domain-specific treatment and is not widely accessible to the ML community. Moreover, the objects (vessels) are small and sparse, challenging traditional computer vision approaches. We present the largest labeled dataset for training ML models to detect and characterize vessels from SAR. xView3-SAR consists of nearly 1,000 analysis-ready SAR images from the Sentinel-1 mission that are, on average, 29,400-by-24,400 pixels each. The images are annotated using a combination of automated and manual analysis. Co-located bathymetry and wind state rasters accompany every SAR image. We provide an overview of the results from the xView3 Computer Vision Challenge, an international competition using xView3-SAR for ship detection and characterization at large scale. We release the data (<https://iuu.xview.us/>) and code (<https://github.com/DIUx-xView>) to support ongoing development and evaluation of ML approaches for this important application.

1

1 Introduction

Recent advances in remote sensing technology have allowed fishing activity to be tracked across the globe via the Automatic Identification System (AIS) which can broadcast vessels’ location [12]. Use of AIS, however, varies by region and fleet; not all vessels are required to carry AIS [29]; some turn their AIS off to engage in illicit activities [23]. This unknown number of non-broadcasting vessels that evade conventional monitoring systems—referred to as “dark” vessels—greatly limits our ability to manage marine resources. Illegal, unreported, and unregulated (IUU) fishing comprises over 20% of all catch around the world [1]. In recent years, the largest IUU fishing offenses were perpetrated by fleets that mostly did not use AIS [23], costing legitimate fishers and governments billions of dollars while also damaging critical ecological systems.

Satellite imagery provides an alternative means of sensing dark vessels. Common electro-optical (EO) satellites, however, are limited by cloud coverage and low light conditions. Synthetic aperture radar (SAR) satellites, on the other hand, are able to image in all weather conditions and at nighttime. The European Space Agency (ESA) Sentinel-1 radar satellites cover all coastal waters around the world approximately every six days, offering open access to the full SAR archive. Despite its availability,

*Equal contribution

†Corresponding author, ritwik.ctr@diu.mil

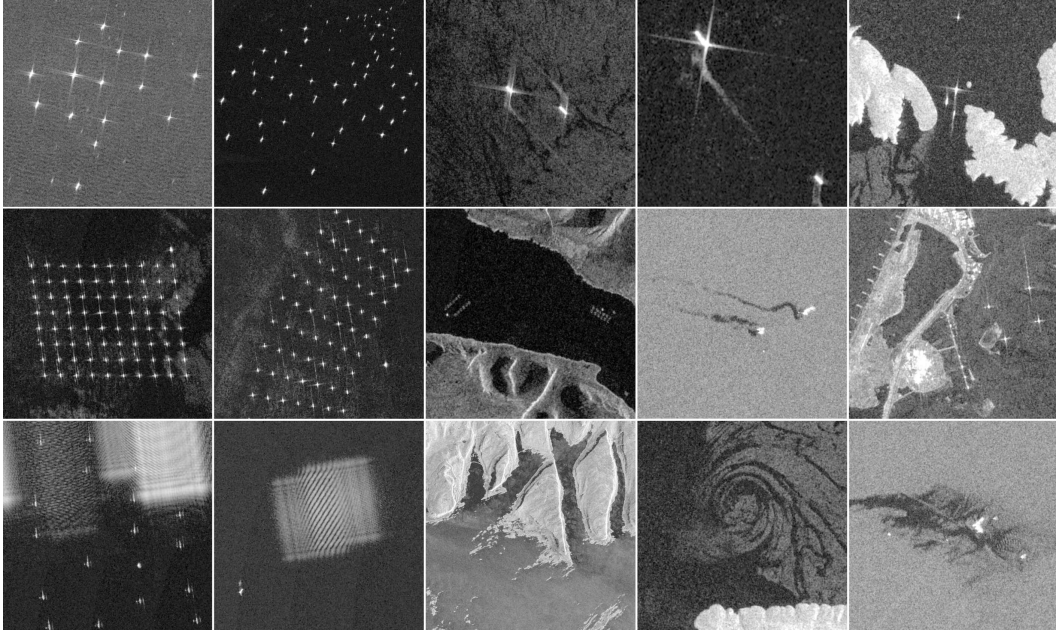


Figure 1: Example of objects and features in xView3-SAR: (top row) vessels of different size, type, and brightness with different backgrounds; (middle row) fixed infrastructure such as wind farms, fish cages, platforms, and port towers; (bottom row) noise artifacts, rough coastlines, rocks, and wind-driven ocean features.

there exist two significant barriers in utilizing Sentinel-1 SAR archive, and SAR images in general, for maritime object detection and characterization using machine learning (ML) models.

The first barrier is creating analysis-ready pixels. SAR actively beams from a moving sensor; these radar waves interact with moving objects on the ground and interfere with themselves, resulting in reconstructed images that contain noise features—speckles and visible discontinuity, for example—even after processing. SAR images can appear distinctly different from RGB images commonly used in ML models today, and interpreting SAR images requires domain expertise. In addition, SAR requires a series of computationally expensive, complex, and domain-specific prepossessing steps [32].¹ These factors greatly limit the access ML practitioners have to analysis-ready SAR pixels.

The second barrier is ground-truthing dark vessels. Dark vessels, by their very nature, actively seek to evade detection. Moreover, vessels are small objects, appearing as a few bright pixels scattered through large areas on a cluttered background. In fact, annotated bounding boxes account for only 0.005% of the image pixels in our dataset, which is in stark contrast with what is commonly encountered in RGB images (e.g., MS-COCO). It is therefore necessary to rely on expert manual inspections *and* additional modalities to identify all objects.

Due to these barriers, existing datasets to support the development of computational models for detecting and characterizing dark vessels are extremely limited in size and scope.

We break these barriers by releasing **xView3-SAR**, the largest dataset of its type by an order of magnitude. We combine: (1) AIS data; (2) a state-of-the-art AIS-SAR matching algorithm; (3) expert human-analyst verification to construct xView3-SAR. It is a multi-modal ship detection and characterization dataset comprised of: (1) 991 analysis-ready Sentinel-1 SAR imagery averaging 29,400-by-24,400 pixels each; (2) 243,018 verified maritime objects in over 43.2 million square kilometers; (3) detailed annotations for a novel multitask problem formulation that reflects the priorities of anti-IUU fishing practitioners; (4) co-located surface wind condition and bathymetry rasters that provide valuable context for the primary tasks; (5) a set of reference code to expedite users’ development process.

¹For a further understanding of SAR, the reader may refer to NASA and ESA sources [10, 20].

Lastly we provide a high-level overview from the results of the xView3 Computer Vision Challenge, an international competition using xView3-SAR to detect and characterize dark vessels at large scale. The Challenge brought awareness of the IUU fishing problem to the wider ML community and resulted in the creation of accurate and efficient models that have been deployed in real-world anti-IUU fishing missions. These models provide a useful benchmark for the ML community and shed light on areas for future research; they highlight the contributions of xView3-SAR in bridging the fields of ML research and remote sensing on the IUU fishing applications.

2 Related Work

Ship detection on satellite imagery is a well-explored problem. A widely used approach for SAR imagery is the Constant False Alarm Rate (CFAR) method [13, 22], which characterizes the statistical properties of the sea clutter to create separation between the background pixels and targets of interest. This statistical characterization can be either theoretical, e.g., defining a probability density function that describes the backscatter properties of the image, or empirical, e.g., computing the local mean and standard deviation of background pixels [9]. [8, 14, 37, 42] propose thresholding, shape, and texture-based methods to identify ships on EO and SAR imagery. [9, 17, 31] implement wavelet transforms and spectral analysis to better separate background from foreground and enable better detection. These conventional approaches, however, require substantial experimentation in order to find the optimal configuration for a specific data type, usually involving human analysts with domain expertise to evaluate the results. These methods do not adapt nor scale well to new environments or satellites and are not robust to “unseen” data artifacts.

More recently, deep learning methods for computer vision have provided a compelling new approach to the ship detection problem [2, 18]. Convolutional neural network architectures have been used, with the most common strategies adopting either a single-stage approach where a pre-defined image grid is scanned and evaluated for object presence on each cell at once [4, 6, 34, 39], or a dual-stage approach where regions of the image are selected for further analysis and then classified in a secondary pass [15, 40]. [7] combines a modified generative adversarial network with a single-stage detector to produce state-of-the-art results for small-ship detection. [30] separates the detection problem into two independent tasks, first utilizing a deep neural network to extract features for ships and then passing those features to a downstream model for classification.

These approaches have been mostly applied to (and developed for) small-scale problems using a limited number of images, partly because large annotated SAR datasets are difficult to construct. It is particularly hard to annotate SAR images with the detail necessary to enable vessel characterization (versus detection) due to the difficulty of fusing SAR imagery with AIS. Approaches to this fusion problem range from correlating AIS pings to ships in a given area and time [19] to projecting a ship’s likely position in a SAR image by interpolating AIS pings [16, 24].

The majority of publicly available datasets for ship detection are based on EO imagery (e.g., [28, 36, 39]), with few available specifically for SAR-based object detection. Some examples include the LS-SSDD-v1.0 [38] providing 15 SAR scenes from Sentinel-1 with 6,015 expert-annotated ship bounding boxes, verified with AIS and Google Earth co-incident imagery where available; and the work of [34] providing 43,819 instances of cropped ship images from 102 Gaofen-3 SAR images, with bounding boxes annotated by human experts.

3 Dataset Construction

We used SAR imagery from ESA Sentinel-1 mission, which comprises two near-polar-orbiting satellites providing 24/7 coverage of all coastal waters approximately every 6 days. SAR satellites can function in many different “acquisition modes,” each with a different primary application and resolution trade-off. We use the Interferometric Wide (IW) swath mode Level-1 Ground Range Detected (GRD) products, which are freely available through ESA and NASA data portals.² The IW mode GRD products include both the vertical-horizontal (VH) and vertical-vertical (VV) polarization bands for each image. The VH band is usually better suited for ship detection due to better separation between vessels and the sea clutter. The VV band is better at identifying sea surface features (e.g., oil

²ESA: <https://scihub.copernicus.eu>; NASA: <https://search.asf.alaska.edu/>. See full description of the product on their websites.

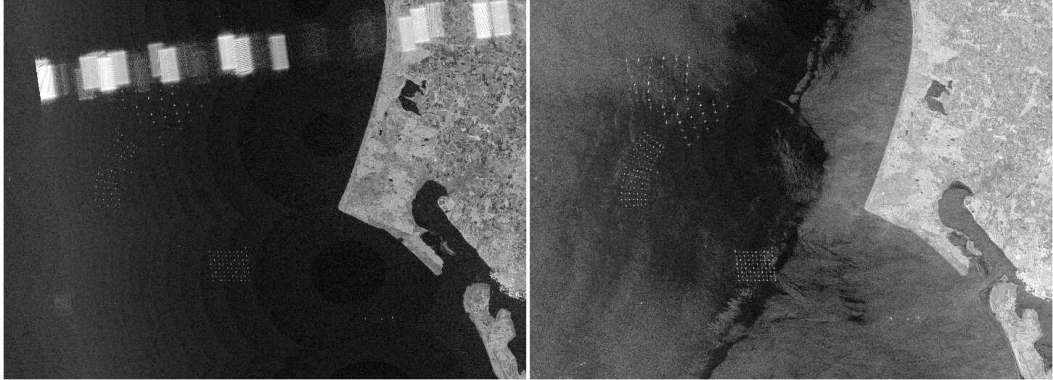


Figure 2: Excerpt of a Sentinel-1 SAR image showing both polarization bands: VH (left) and VV (right). Note how different features appear on each band, e.g., a strong radar interference artifact is visible in the VH band, and wind-driven features on the ocean surface are visible in the VV band. Both bands depict clearly the patterns of fixed infrastructure (likely wind farms). Location is near Esbjerg, Denmark.

slicks, sediment plumes, wind features) that provide useful context for ship characterization. They have a spatial resolution of about 20 meters and a pixel spacing of 10-by-10 meters. Note that small vessels appearing as single pixels may have high backscatter intensities, resulting in a diffusion effect that allows sub-pixel detection and characterization (see Figure 1 row 1, column 1).

We constructed the xView3-SAR dataset by following a series of steps: (1) select strategic geographic areas; (2) process the raw imagery; (3) process the ancillary data; (4) detect objects with an automated CFAR algorithm; (5) correlate AIS data to SAR detections; (6) classify AIS data to characterize vessel type and activity; (7) manually label images; (8) combine manual and automated annotations; (9) partition the data for training and validating ML algorithms. Each of these steps are described in detail below.

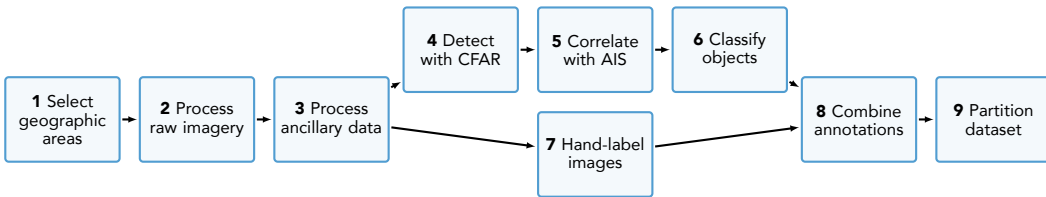


Figure 3: Dataset creation process; see Section 3 for more details.

Step 1. Select geographic areas. Capturing diversity in geographic areas and therefore vessel types, traffic patterns, latitudes, and a variety of fixed infrastructure, was a prioritized design decision for xView3-SAR (Figure 4). We include several areas near Europe because many European vessels broadcast their GPS positions, which serve as an abundant source of high confidence, matched labels for SAR imagery. These regions include the North Sea, Bay of Biscay, Iceland, and the Adriatic Sea. We also include images from West Africa which are regions with high IUU activity and substantial oil development. The inclusion of these images increases the number of fixed infrastructure platforms in the dataset and creates a more challenging environment for vessel identification. In all, the xView3-SAR dataset is built from 991 SAR images that are, on average, 29,400-by-22,400 pixels. It is important to note that xView3-SAR does not offer a true global coverage and therefore may not represent all vessel distributions.

Step 2. Process raw images. Raw Sentinel-1 imagery require a series of computationally-intensive and domain-specific processing steps to create consistent, ML-ready rasters. We used the Sentinel-1 Toolbox³ to derive backscatter values (in dB) for each pixel from the original unprojected GRD products. This includes orbit correction, removal of noise artifacts, radiometric calibration, terrain

³<https://step.esa.int/main/toolboxes/snap/>

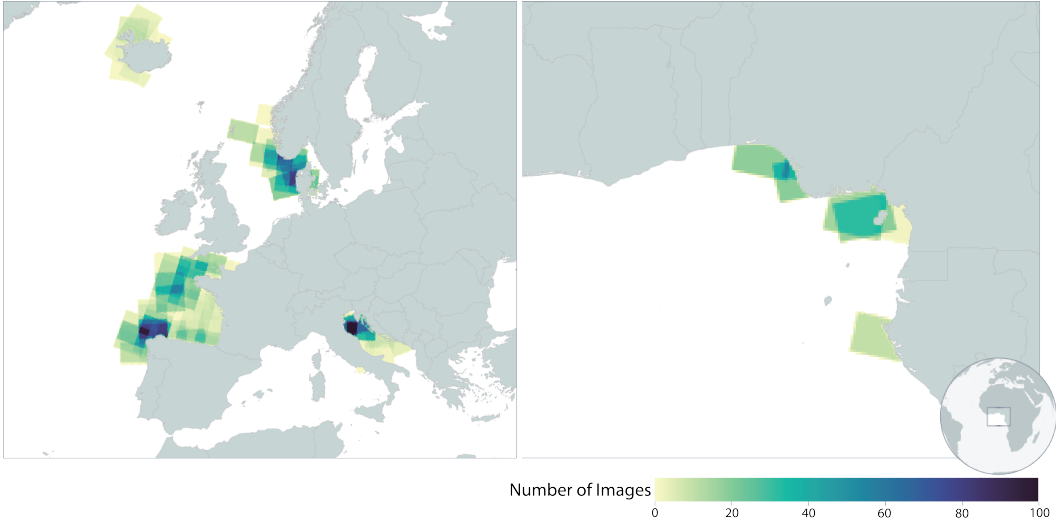


Figure 4: Geographic distribution of Sentinel-1 images used in the xView3 dataset. (left) European waters present a diversity of maritime objects, such as fishing and shipping vessels of all sizes, and offshore infrastructure. (right) The west coast of Africa is known to have large IUU activity.

correction, and reprojection to the WGS84 reference system [21]. Lastly, we reproject and provide all images in UTM projection, with 10-meter pixel spacing for the VH and VV rasters. The rasters are distributed as GeoTIFFs with an original file size of approximately 2.4 GB per band. We use half-precision floating point to facilitate data download, resulting in 50% decreased file sizes.

Step 3. Process ancillary data. In addition to the VH and VV SAR images, we provide a set of ancillary rasters to aid the ship detection task and support novel approaches in creating context-aware analytical models (Figure 11). Sentinel-1 Level-2 Ocean (OCN) products are available in lower resolution with a pixel spacing of 1 kilometer; they were also reprojected to WGS84. The bathymetry product obtained from the General Bathymetric Chart of the Oceans [5] consists of a global terrain model on a 15 arc-second interval grid in WGS84; we clipped it to match the extent of each SAR image. All ancillary data is reprojected to 500-meter pixel spacing. Overall, ancillary data includes bathymetry, wind speed and direction, wind quality, and land/ice masks. We selected only SAR images for which corresponding ancillary rasters were available.

Step 4. Detect objects automatically. Global Fishing Watch (GFW) maintains an extensive database of vessels and offshore infrastructure derived from Sentinel-1 imagery [35]. The detection approach combines a well-established CFAR ship detection method [27, 33] with a modern ML classification model to identify and filter out noise and estimate length. For xView3-SAR, we selected over 161,000 detections from 2020 spread over several geographic areas.

Step 5. Correlate AIS to automated detections. GFW also maintains an extensive database of processed AIS data [29]. Matching AIS messages to the respective vessels on SAR images is challenging, because the time of each AIS record does not coincide with the image collection time. We utilize a probabilistic model that determines {AIS, SAR-detection} pairs based on AIS records before and after the time of the image and the probability of matching to any of the vessels on that image [11]. This step is crucial in providing labeled data for training and testing ML models, as well as to validating external labeling protocols.

Step 6. Classify AIS to characterize vessels. We supplement matched detections with GFW’s estimates of vessel type and activity (i.e., fishing vs. non-fishing). These identities were determined by combining information from available vessel registries with predictions from an artificial neural network [12] that analyzes vessel movement patterns to estimate vessel type and activity.

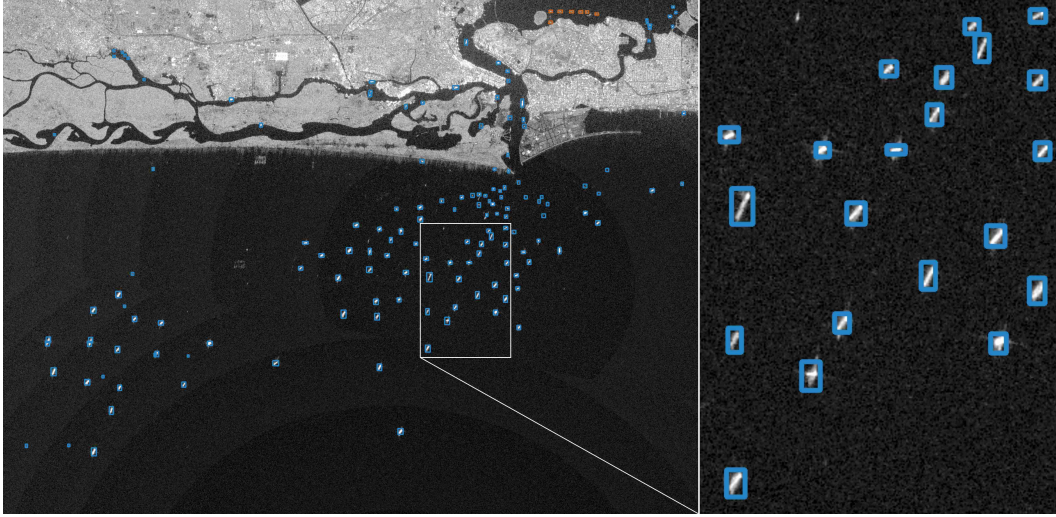


Figure 5: A Sentinel-1 SAR view near Lagos, Nigeria, showing bounding boxes of detected vessels (blue) and fixed infrastructure (orange, top right corner on left panel). Note the characteristic SAR speckle noise in the background (zoom in, right panel).

Step 7. Detect objects manually. We trained professional labelers to visually identify the bounds and the category of objects in 437 SAR images. These manual annotations provided approximately 176,000 labeled detections, along with the annotator’s confidence in identifying the objects. Our instructions to labelers are provided in the Appendix F.

Step 8. Combine automated and manual annotations. Our labeling approach is unique, as we bring together both AIS information and expert analysts to provide a comprehensive labeling system. Many instances of hand labels were also labeled by GFW’s automated approach, while some instances were unique new labels (due to, e.g., the inability of the current GFW algorithm to detect vessels close to shore). By correlating AIS information with information provided by human annotators, we are able to assign confidence levels—high, medium, low—to each label (see Appendix Section A for more details). Overall, we generated 243,018 labels, with 39.1% having both automated and manual annotations, 27.5% automated only, and 33.4% manual only.

Step 9. Partition the data. For the xView3 Computer Vision Challenge, we partitioned the data into four sets: *train*, 554 images; *validation*, 50 images; *public*, 150 images; *holdout*, 237 images. The *train* set contains only automated GFW labels only whereas all other sets contain labels created by combining GFW automated annotation and manual annotation.⁴ The *train* and *validation* sets were provided to competitors for training and evaluating their ML models; the *public* set was used for the in-challenge public leaderboard; the *holdout* set was retained for final model performance assessment. We release all data but the *holdout* set.

4 xView3 Computer Vision Challenge

The xView3-SAR dataset was developed for the xView3 Computer Vision Challenge, an international competition to detect and characterize dark vessels using computer vision and global SAR satellite imagery. The competition, led by the U.S. Defense Innovation Unit and GFW, launched on August 2021. Over 2,000 competitors used xView3-SAR to develop state-of-the-art maritime object detection and characterization algorithms. The Challenge aimed to deploy selected algorithms to support real-world practitioners in the fight against IUU fishing. Below, we describe the ML tasks in the xView3 Challenge using xView3-SAR. While a full analysis of the winning models from the Challenge is beyond the scope of this paper, we offer some observations that future users of xView3-SAR may find useful in section 4.3.

⁴See Tables 2 and 3 in Appendix B for the breakdowns of the geographical and automated/manual annotation distribution for each data partition.

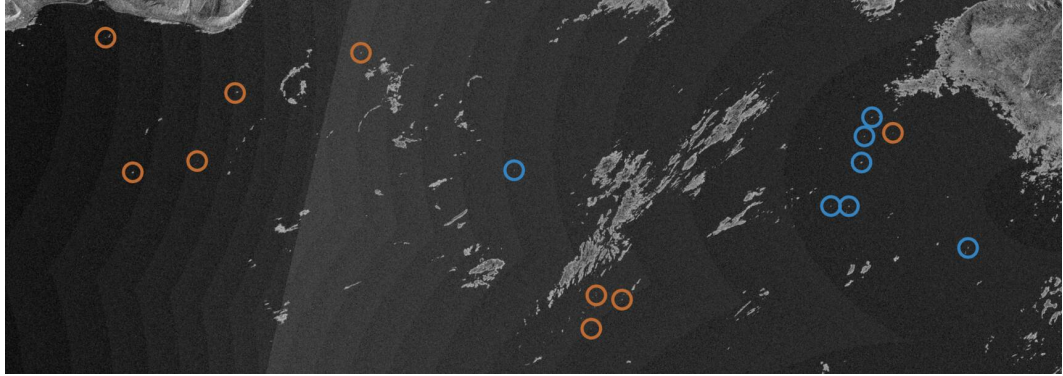


Figure 6: Example of mixed annotations along a complex shoreline in northwest Iceland. Blue circles are high confidence human annotations correlated with AIS information; orange circles are AIS-only annotations. This is a challenging scenario for vessel detection as many rocks can be confounded with real objects.

4.1 ML tasks and evaluation

Maritime Object Detection. To evaluate detection performance, the Challenge considered “ground truth positives” to be human-made maritime objects in an image that were either (1) identified as a human-made object by a human labeler with high or medium confidence and/or (2) identified via a high confidence correlation with AIS. Difficult aspects of this task included: (1) detailed shoreline mapping; (2) handling SAR artifacts such as ambiguities and sea clutter; (3) maintaining high performance across sea states, satellite configurations, and geographic domains. The Challenge used the F1 score over all maritime objects, $F1_D$, to measure performance on this task.

Close-to-Shore Object Detection. This is of particular interest because there is a higher density of vessels closer to shore, and they can be difficult to differentiate from small islands or shoreline features. Moreover, when vessels are close together, radar signals that interact with vessels can also interact with surrounding land and structures. Other human-made objects, such as piers or bridges, are also common. The Challenge used an F1-score, $F1_S$, that compared predictions that are within two kilometers from shore to ground truth detections in those areas, where pixel-level shorelines for each SAR image were computed by finding the 0-meter contour on the co-registered bathymetry map.

Vessel Classification. This task determines whether a maritime object is a “vessel” or “non-vessel.” Non-vessels are fixed infrastructure such as offshore wind turbines, oil rigs, or fish farms. For evaluation purposes, the Challenge considered “ground truth positives” to be vessels in an image that were either (1) identified as a vessel by a human labeler with high or medium confidence and/or (2) identified as a vessel via correlation with AIS. A standard F1 score over detections for which vessel information was available, $F1_V$, was used to measure performance on this task.

Fishing Classification. Solvers were asked to further break down the “vessel” class into “fishing” and “non-fishing” classes. The Challenge used standard a standard F1 score, $F1_F$, to measure performance on this task, with positives defined as vessels in the “fishing” class. Ground truth labels for this task came from both (1) reported AIS data and (2) the AIS analysis algorithm of [12], which is 99% accurate at classifying a vessel as “fishing” or “non-fishing” based on AIS information. The $F1_F$ metric considers annotations for which AIS information was available. Fishing classification annotations represent a substantial contribution of xView3-SAR.

Vessel Length Estimation. Vessel size is a valuable piece of information to anti-IUU practitioners. The Challenge defined performance on this regression task using an “aggregate percent error,” PE_L :

$$PE_L = 1 - \min \left(\frac{1}{N} \sum_{n=1}^N \frac{|\min(\hat{\ell}_n, \ell_{\max}) - \min(\ell_n, \ell_{\max})|}{\min(\hat{\ell}_n, \ell_{\max})}, 1 \right), \quad (1)$$

Rank	Competitor	Aggregate	$F1_D$	$F1_S$	$F1_V$	$F1_F$	PE_L
1	BloodAxe	0.6177	0.7702	0.5310	0.9392	0.8425	0.6971
2	selim_sef	0.6047	0.7629	0.4768	0.9346	0.8079	0.7437
3	Tumen	0.5805	0.7395	0.4205	0.9479	0.8279	0.7289
4	Skylight at AI2	0.5777	0.7322	0.4674	0.9293	0.8232	0.7253
5	Kohei	0.5717	0.7342	0.4527	0.9380	0.7910	0.7112
	xView3 reference model	0.1904	0.4302	0.1293	0.6891	0.3946	0.0000

Table 1: Results of the xView3 Challenge on the *holdout* partition. Note that the xView3 reference model was a simple Faster-RCNN that naively estimated length in a way that led to large percent error.

where ℓ is the true length and $\hat{\ell}$ the predicted length; ℓ_{\max} is the maximum length of a predicted or ground truth object.⁵

Overall Ranking Metrics. The Challenge combined individual performance metrics to compute an aggregate multitask metric M_R to rank submissions to the Challenge. M_R was designed such that: (1) scores should range between zero and one; (2) poor overall maritime object detection should result in poor overall performance; (3) advances on any of the other tasks should result in equal levels of score improvement:

$$M_R = F_D \times \frac{1 + F1_S + F1_V + F1_F + PE_L}{5}. \quad (2)$$

Evaluation Constraints. We aimed to deploy the winning Challenge models to aid the real-world anti-IUU efforts. Since anti-IUU practitioners often operate under limited computing resources and time is critical, a useful model must be computationally efficient. Concretely, competitors were asked to create models that can run inference on any full SAR image, averaging of 29,400-by-24,400 pixels, in 15 minutes on a computer with one Tesla V100 GPU, 60 GB RAM, and a server-grade CPU.

4.2 Reference model

To introduce the xView3-SAR dataset and associated ML tasks, a reference detection and classification model was provided. This model is based on Faster-RCNN [25] and serves as a starting point upon which users could build. We describe this approach in detail in Appendix C. Note that the reference model is provided on the [xView3 GitHub repository](#) in order to allow the community to make the most effective use of the dataset. Code for implementation of the above metrics—which we consider a substantial contribution—is also provided.

4.3 Summary of xView3 Challenge Results

The xView3 Challenge ran from August to November, 2021. During this period, competitors submitted their predictions on the *public* set. At the conclusion of the challenge, competitors’ models were evaluated against the *holdout* set (Table 1). Competitors adopted creative ML strategies to tackle the object detection, classification, and regression tasks. This section provides a high-level overview of the top-performing models, leaving detailed analyses to future researchers.⁶

Top solutions generally adopted single-stage object detection models tailored for predicting small, tightly packed objects. Single-stage object detection models allow for efficient inference to abide by the inference runtime limit. The first place model uses pre-trained CircleNets [41] for the encoder and U-Net [26] as the decoder to produce an intermediate feature map that is then operated upon by the model head. The model head predicts an objectness map, offset length, and two dense classification labels—whether the object in question is a vessel and, if so, whether it is a fishing vessel. The regression head was modified to predict only the object length (in pixels).

Data augmentation specific to the SAR domain is addressed by all top solutions. This is significantly more challenging than for RGB images because the set of valid image augmentations is limited.

⁵ ℓ_{\max} is set as 500, in meters, to bound the maximum potential error. The number is chosen based on the largest known vessel, [Seawise Giant](#).

⁶ Interested readers can visit xView3 GitHub repository, <https://github.com/DIUx-xView>, which contains code and detailed reports for each of the winning solutions.

Competitors extended the Albumentations library [3] to include several custom-made augmentations tailored for SAR. These changes include, e.g., random brightness and contrast changes and various noise additions to mimic different speckle patterns. Additionally, competitors explored strategies to remove artifacts from the SAR imagery processing pipeline, such as apodization in discrete Fourier space to remove diffraction spikes near strong reflectors (as seen in Figure 1’s top row).

All models struggled with predicting vessels accurately near the shoreline (see Table 1, $F1_S$). Since shorelines are rocky, uneven, and full of odd surfaces, SAR effects such as multi-path effects and scattering are much more common near the shoreline. No competitor developed specific methods to account for the shoreline effect.

The combination of novel single-stage detectors, imbalanced class training, data augmentation strategies, and more resulted in marked improvements in accuracy and runtime performance over competitors who did not employ any such strategies. Detailed documentations for the top five solutions can be found on the xView3 Github repository.⁷

The final competition leaderboard and additional resources are available on the [xView3 Challenge website](#); we intend to allow ongoing submissions to the leaderboard. All code and weights for the top five machine learning solutions are released as [open source code](#), and each is accompanied by a descriptive report. These resources will enable follow-on research using xView3-SAR.

5 Conclusion & Future Work

IUU fishing is an urgent problem causing immense harm to our marine biosphere. Understanding the nature and the locations of IUU fishing is a difficult problem, one that is further complicated by limited enforcement resources. Technology to efficiently, accurately, and rapidly identify vessels engaged in IUU fishing is therefore critical to the long-term health of global fisheries.

SAR imagery and automated ML-based algorithms can serve as a powerful tool to find and characterize vessels engaged in IUU fishing. Enabling automated detections of dark vessels in millions of square kilometers of imagery covering the world’s waters will make international agencies, partners, and allies much more effective at protecting the oceans.

To do so, we have constructed and released xView3-SAR. The dataset covers 43.2 million square kilometers in 991 SAR images averaging 29,400-by-24,400 pixels each. It contains AIS and human-verified labels for ship detection and characterization. Importantly, the labels provide crucial characteristics and information to anti-IUU practitioners. The xView3-SAR dataset is the largest of its kind by an order of magnitude. The xView3 Challenge, using xView3-SAR, brought awareness of the IUU fishing problem to the wider ML community and enabled it to create accurate and efficient models that perform the detection, classification, and length estimation tasks that international agencies, partners, and allies need to act against IUU fishing.

Toolchains and utilities based on xView3-SAR and the xView3 Challenge have already been deployed to support both government and non-governmental organizations in their ongoing anti-IUU missions, highlighting our contribution in bridging fields of ML and remote sensing.

xView3-SAR and the xView3 Challenge have unlocked the potential for combining ML and remote sensing in the fight against IUU-fishing. With the aid of xView3-SAR, advancements in multi-scale representation learning, contextually aware models, resource-efficient computer vision, positive-unlabeled learning, and the use of auxiliary modalities represent compelling areas for future work. By demonstrating the effectiveness of ML on large quantities of SAR imagery—and by providing the xView3-SAR dataset and winning models from the xView3 Challenge—we hope to spur research to advance the state-of-the-art and to allow us to leverage the unique capabilities of SAR imaging technology to combat IUU fishing.

References

[1] David J. Agnew, John Pearce, Ganapathiraju Pramod, Tom Peatman, Reg Watson, John R. Beddington, and Tony J. Pitcher. Estimating the Worldwide Extent of Illegal Fishing. *PLOS*

⁷While thorough analysis of the top solutions is beyond the scope of this paper, we nonetheless believe future researchers would find a more details description of the first place model useful; it is included in Appendix D.

ONE, 4(2):e4570, Feb. 2009. 1

[2] George Barbastathis, Aydogan Ozcan, and Guohai Situ. On the use of deep learning for computational imaging. *Optica*, 6(8):921–943, Aug. 2019. 3

[3] Alexander Buslaev, Alex Parinov, Eugene Khvedchenya, Vladimir I. Iglovikov, and Alexandr A. Kalinin. Albumentations: Fast and flexible image augmentations. *Information*, 11(2):125, Feb. 2020. 9

[4] Tobias Carman and Avyaya Kolhatkar. A comparison of fixed threshold CFAR and CNN ship detection methods for S-band NovaSAR images. *Small Satellite Conference*, Aug. 2020. 3

[5] British Oceanographic Data Centre. GEBCO 2020 Grid. 5

[6] Yang-Lang Chang, Amare Anagaw, Lena Chang, Yi Chun Wang, Chih-Yu Hsiao, and Wei-Hong Lee. Ship detection based on YOLOv2 for SAR imagery. *Remote Sensing*, 11(7):786, Jan. 2019. 3

[7] Zhijun Chen, Depeng Chen, Yishi Zhang, Xiaozhao Cheng, Mingyang Zhang, and Chaozhong Wu. Deep learning for autonomous ship-oriented small ship detection. *Safety Science*, 130:104812, Oct. 2020. 3

[8] Christina Corbane, Laurent Najman, Emilien Pecoul, Laurent Demagistri, and Michel Petit. A complete processing chain for ship detection using optical satellite imagery. *International Journal of Remote Sensing*, 31(22):5837–5854, Dec. 2010. 3

[9] D. J. Crisp. The State-of-the-Art in Ship Detection in Synthetic Aperture Radar Imagery., 2004. 3

[10] ESA. Sentinel-1 SAR User Guide. <https://sentinels.copernicus.eu/web/sentinel/user-guides/sentinel-1-sar>. 2

[11] David Allen Kroodsma, Tim Hochberg, Pete Davis, Fernando Paolo, Rocio Joo, and Brian Adrian Wong. Revealing the Global Longline Fleet with Satellite Radar. Apr. 2022. 5

[12] David A. Kroodsma, Juan Mayorga, Timothy Hochberg, Nathan A. Miller, Kristina Boerder, Francesco Ferretti, Alex Wilson, Bjorn Bergman, Timothy D. White, Barbara A. Block, Paul Woods, Brian Sullivan, Christopher Costello, and Boris Worm. Tracking the global footprint of fisheries. *Science*, 359(6378):904–908, Feb. 2018. 1, 5, 7

[13] Xiangguang Leng, Kefeng Ji, Kai Yang, and Huanxin Zou. A Bilateral CFAR Algorithm for Ship Detection in SAR Images. *IEEE Geoscience and Remote Sensing Letters*, 12(7):1536–1540, July 2015. 3

[14] Ge Liu, Yafen Zhang, Xinwei Zheng, Xian Sun, Kun Fu, and Hongqi Wang. A new method on inshore ship detection in high-resolution satellite images using shape and context information. *IEEE Geoscience and Remote Sensing Letters*, 11(3):617–621, Mar. 2014. 3

[15] Zikun Liu, Jingao Hu, Lubin Weng, and Yiping Yang. Rotated region based CNN for ship detection. In *2017 IEEE International Conference on Image Processing (ICIP)*, pages 900–904, Sept. 2017. 3

[16] Gerard Margarit, José A. Barba Milanés, and Antonio Tabasco. Operational ship monitoring system based on synthetic aperture radar processing. *Remote Sensing*, 1(3):375–392, Sept. 2009. 3

[17] Armando Marino, Maria J. Sanjuan-Ferrer, Irena Hajnsek, and Kazuo Ouchi. Ship detection with spectral analysis of synthetic aperture radar: A comparison of new and well-known algorithms. *Remote Sensing*, 7(5):5416–5439, May 2015. 3

[18] Morgan P. McBee, Omer A. Awan, Andrew T. Colucci, Comeron W. Ghobadi, Nadja Kadom, Akash P. Kansagra, Srinivasa Tridandapani, and William F. Auffermann. Deep Learning in Radiology. *Academic Radiology*, 25(11):1472–1480, Nov. 2018. 3

[19] Aristides Milios, Konstantina Bereta, Konstantinos Chatzikolakis, Dimitris Zissis, and Stan Matwin. Automatic fusion of satellite imagery and AIS data for vessel detection. In *2019 22th International Conference on Information Fusion (FUSION)*, pages 1–5, July 2019. 3

[20] NASA Earth Data. What is Synthetic Aperture Radar. <https://earthdata.nasa.gov/learn/backgrounders/what-is-sar/>, Apr. 2020. 2

[21] National Geospatial-Intelligence Organization. World Geodetic System 1984. Technical report. 5

[22] Odysseas Pappas, Alin Achim, and David Bull. Superpixel-Level CFAR Detectors for Ship Detection in SAR Imagery. *IEEE Geoscience and Remote Sensing Letters*, 15(9):1397–1401, Sept. 2018. 3

[23] Jaeyoon Park, Jungsam Lee, Katherine Seto, Timothy Hochberg, Brian A. Wong, Nathan A. Miller, Kenji Takasaki, Hiroshi Kubota, Yoshiaki Oozeki, Sejal Doshi, Maya Midzik, Quentin Hanich, Brian Sullivan, Paul Woods, and David A. Kroodsma. Illuminating dark fishing fleets in North Korea. *Science Advances*, 6(30):eabb1197, July 2020. 1

[24] Ramona Pelich, Marco Chini, Renaud Hostache, Patrick Matgen, Carlos Lopez-Martinez, Miguel Nuevo, Philippe Ries, and Gerd Eiden. Large-scale automatic vessel monitoring based on dual-polarization sentinel-1 and AIS data. *Remote Sensing*, 11(9):1078, Jan. 2019. 3

[25] Shaoqing Ren, Kaiming He, Ross Girshick, and Jian Sun. Faster R-CNN: Towards Real-Time Object Detection with Region Proposal Networks. In *Advances in Neural Information Processing Systems*, volume 28. Curran Associates, Inc., 2015. 8, 2

[26] Olaf Ronneberger, Philipp Fischer, and Thomas Brox. U-Net: Convolutional Networks for Biomedical Image Segmentation. *arXiv:1505.04597 [cs]*, May 2015. 8

[27] Louis L. Scharf. *Statistical Signal Processing: Detection, Estimation, and Time Series Analysis*. Addison-Wesley Pub. Co, Reading, Mass, 1990. 5

[28] Zhenfeng Shao, Wenjing Wu, Zhongyuan Wang, Wan Du, and Chengyuan Li. SeaShips: A large-scale precisely annotated dataset for ship detection. *IEEE Transactions on Multimedia*, 20(10):2593–2604, Oct. 2018. 3

[29] M. Taconet, D. Kroodsma, and J. A. Fernandes. Global atlas of AIS-based fishing activity: Challenges and opportunities. Technical report, FAO, 2019. 1, 5

[30] Jierong Tang, Chenwei Deng, Guang-Bin Huang, and Baojun Zhao. Compressed-domain ship detection on spaceborne optical image using deep neural network and extreme learning machine. *IEEE Transactions on Geoscience and Remote Sensing*, 53(3):1174–1185, Mar. 2015. 3

[31] M. Tello, C. Lopez-Martinez, and J.J. Mallorqui. A novel algorithm for ship detection in SAR imagery based on the wavelet transform. *IEEE Geoscience and Remote Sensing Letters*, 2(2):201–205, Apr. 2005. 3

[32] Michele Vespe and Harm Greidanus. SAR Image Quality Assessment and Indicators for Vessel and Oil Spill Detection. *IEEE Transactions on Geoscience and Remote Sensing*, 50:4726–4734, Apr. 2012. 2

[33] Chao Wang, Shaofeng Jiang, Hong Zhang, Fan Wu, and Bo Zhang. Ship Detection for High-Resolution SAR Images Based on Feature Analysis. *IEEE Geoscience and Remote Sensing Letters*, 11(1):119–123, Jan. 2014. 5

[34] Yuanyuan Wang, Chao Wang, Hong Zhang, Yingbo Dong, and Sisi Wei. A SAR dataset of ship detection for deep learning under complex backgrounds. *Remote Sensing*, 11(7):765, Jan. 2019. 3

[35] Brian A. Wong, Christian Thomas, and Patrick Halpin. Automating offshore infrastructure extractions using synthetic aperture radar & google earth engine. *Remote Sensing of Environment*, 233:111412, Nov. 2019. 5

[36] Gui-Song Xia, Xiang Bai, Jian Ding, Zhen Zhu, Serge Belongie, Jiebo Luo, Mihai Datcu, Marcello Pelillo, and Liangpei Zhang. DOTA: A large-scale dataset for object detection in aerial images. In *2018 IEEE/CVF Conference on Computer Vision and Pattern Recognition*, pages 3974–3983, Salt Lake City, UT, June 2018. IEEE. 3

[37] Guang Yang, Bo Li, Shufan Ji, Feng Gao, and Qizhi Xu. Ship detection from optical satellite images based on sea surface analysis. *IEEE Geoscience and Remote Sensing Letters*, 11(3):641–645, Mar. 2014. 3

[38] Tianwen Zhang, Xiaoling Zhang, Xiao Ke, Xu Zhan, Jun Shi, Shunjun Wei, Dece Pan, Jianwei Li, Hao Su, Yue Zhou, and Durga Kumar. LS-SSDD-v1.0: A deep learning dataset dedicated to small ship detection from large-scale sentinel-1 SAR images. *Remote Sensing*, 12(18):2997, Jan. 2020. 3

[39] Yuanlin Zhang, Yuan Yuan, Yachuang Feng, and Xiaoqiang Lu. Hierarchical and robust convolutional neural network for very high-resolution remote sensing object detection. *IEEE Transactions on Geoscience and Remote Sensing*, 57(8):5535–5548, Aug. 2019. 3

[40] Zenghui Zhang, Weiwei Guo, Shengnan Zhu, and Wenxian Yu. Toward arbitrary-oriented ship detection with rotated region proposal and discrimination networks. *IEEE Geoscience and Remote Sensing Letters*, 15(11):1745–1749, Nov. 2018. 3

[41] Xingyi Zhou, Dequan Wang, and Philipp Krähenbühl. Objects as Points. *arXiv:1904.07850 [cs]*, Apr. 2019. 8

[42] Changren Zhu, Hui Zhou, Runsheng Wang, and Jun Guo. A novel hierarchical method of ship detection from spaceborne optical image based on shape and texture features. *IEEE Transactions on Geoscience and Remote Sensing*, 48(9):3446–3456, Sept. 2010. 3

xView3-SAR: Detecting Dark Fishing Activity Using Synthetic Aperture Radar Imagery

Supplementary Material

A Label Confidence Levels

We use the following criteria to assign label confidence levels:

- If both the GFW algorithm and professional labelers agreed that an object is a `vessel`, then the object is assigned a label of `vessel` with `HIGH` confidence.
- If the GFW algorithm determined an object is a `vessel` and the professional labelers did not, then the object is `vessel` of `MEDIUM` confidence.
- If the professional labelers determined an object is a `vessel` with `HIGH` or `MEDIUM` confidence and GFW did not, then the object is `vessel` of `MEDIUM` confidence.
- If the professional labelers determined an object is a `vessel` with `LOW` confidence and GFW did not, then the object is `vessel` of `LOW` confidence.
- If the GFW algorithm determines an object to be `non-vessel` and the object is more than 2 kilometers away from shore, then the object is assigned a label of `non-vessel` with `HIGH` confidence.
- If the professional labelers determined an object is a `non-vessel` with `HIGH` confidence and GFW did not, then the object is `non-vessel` of `MEDIUM` confidence.

B Geographical and Annotation Distribution

	Data partition	Region name	Num. of scenes
Train	Adriatic	66	
	Bay of Biscay	315	
	Gulf of Guinea	62	
	Iceland	13	
Validation	Norway	98	
	Adriatic	11	
	Gulf of Guinea	16	
	Iceland	2	
Public	Norway	21	
	Adriatic	42	
	Gulf of Guinea	36	
	Iceland	8	
Holdout	Norway	64	
	Adriatic	57	
	Gulf of Guinea	65	
	Iceland	18	
	Norway	97	

Table 2: Breakdown of the geographic distribution of xView3-SAR.

Data partition	Label source	Percent
Train	AIS	100.00
	AIS	0.91
Validation	AIS/Manual	57.36
	Manual	41.73
Public	AIS	1.73
	AIS/Manual	51.00
Holdout	Manual	47.27
	AIS	1.67
Holdout	AIS/Manual	53.48
	Manual	44.84

Table 3: xView3-SAR label source.

	Train	Validation	Public	Holdout
True	56.74	62.20	64.52	63.02
False	26.04	37.18	34.33	35.98
Not available	17.23	0.62	1.15	1.00

Table 4: Distribution of `is_vessel` labels, percentage of total detections.

C Reference Detection Approach

The reference implementation leverages the Faster-RCNN architecture [25]. The model backbone is initialized using pretrained weights from the ImageNet database. The first layer is replaced by a newly initialized convolutional layer with the appropriate number of input channels. The classification head is adjusted to handle the number of classes used by the model—three in the reference implementation case. Data is preprocessed by dividing each scene into 800 x 800 pixel chips, normalizing pixel values between 0 and 1 at the chip level, and creating a bounding box of 10 pixels on each side and a detection at its centroid for each ground-truth annotation. Each bounding box was provided a label of "non-vessel," "non-fishing vessel," or "fishing vessel." The normalized image is provided as input to the Faster-RCNN backbone, which can be trained as usual given the combination of bounding box and multiclass information provided for each detection.

The reference model is trained for five epochs on an NVIDIA DGX-1 using a single V100 GPU. Stochastic gradient descent with momentum is used to optimize the model with $\alpha = 5e^{-3}$, momentum of 0.9, and weight decay of $5e^{-4}$. A step learning rate scheduler is used with step size = 3 and $\gamma = 0.1$.

When evaluated against the *holdout* split, model scores for each of the tasks (described above) were as follows: $F1_D = 0.4302$ (object detection), $F1_S = 0.1293$ (close-to-shore detection), $F1_V = 0.6891$ (vessel classification), $F1_F = 0.3946$ (fishing classification), and $PE_L = 0.0000$ (length regression) for an aggregate score of 0.1904.

	Train	Validation	Public	Holdout
True	19.51	5.00	5.75	5.40
False	37.22	15.24	11.44	11.47
Not available	43.26	79.76	82.81	83.13

Table 5: Distribution of `is_fishing` labels, percentage of total detections.

Data partition	Percent
Train	70.66
Validation	36.42
Public	34.06
Holdout	32.74

Table 6: Percentage of labels with vessel length.

Note that the reference model makes no attempt to accurately predict lengths. This was implemented solely to demonstrate the required prediction output and test the computation of the metrics. For every detection centroid a square bounding box of fixed width was created, the diagonal of which was used as the predicted length of the vessel.

D Winning Model Performance Overview

We present a brief analysis of winning model detection performance along axes of geography and vessel size. In Figure 13, we see that—as expected—detection models tend to improve as the true vessel size becomes larger. Importantly, in this figure we present metrics computed only vessels for which have a label of either medium or high confidence. While many of the regions behave similarly, it is worth noting that smaller vessels appear harder to find on SAR in the Adriatic than in other areas; this may be due to more common non-metal construction in this region. High recall in the Gulf of Guinea across vessel sizes is also compelling, as this is a high-priority region for IUU activity. Finally, Figure 14 presents the distribution of ground-truth vessels in by size; while there are subtle differences between the different regions, overall the distributions skew strongly right, as one would expect.

E Supplementary Figures

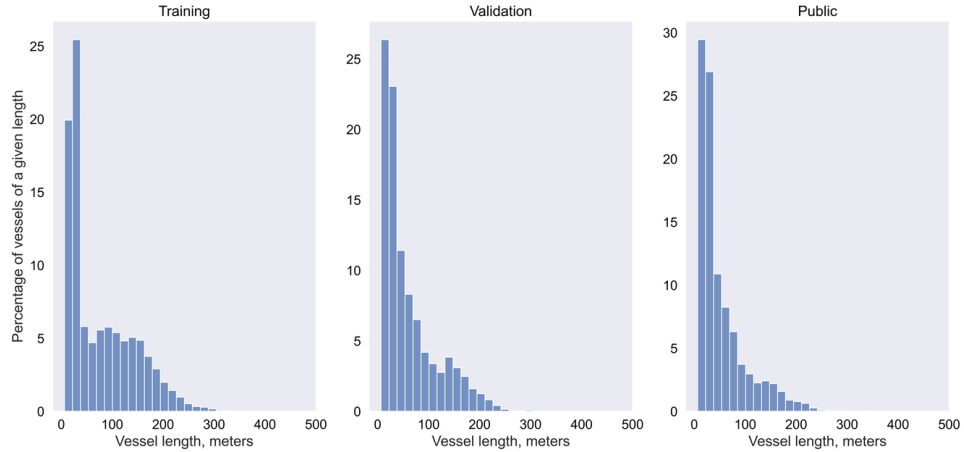


Figure 7: Distribution of vessel lengths.

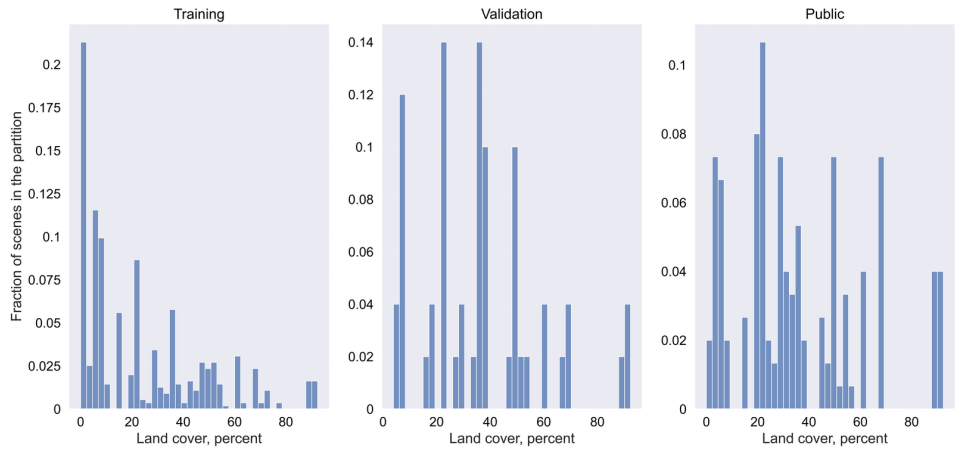


Figure 8: Distribution of land cover. From left to right: train, validation, public test, holdout.

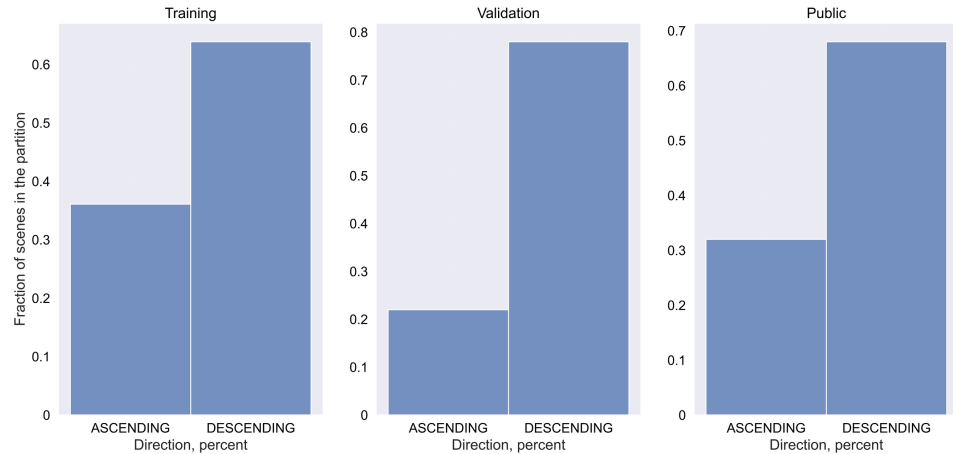


Figure 9: Distribution of satellite direction. From left to right: train, validation, public test, holdout.

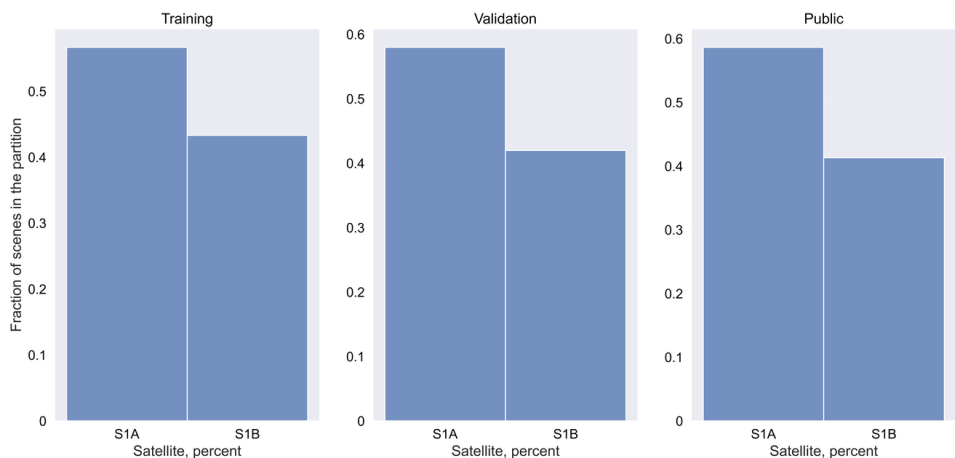


Figure 10: Distribution of satellite instrument source. From left to right: train, validation, public test, holdout.

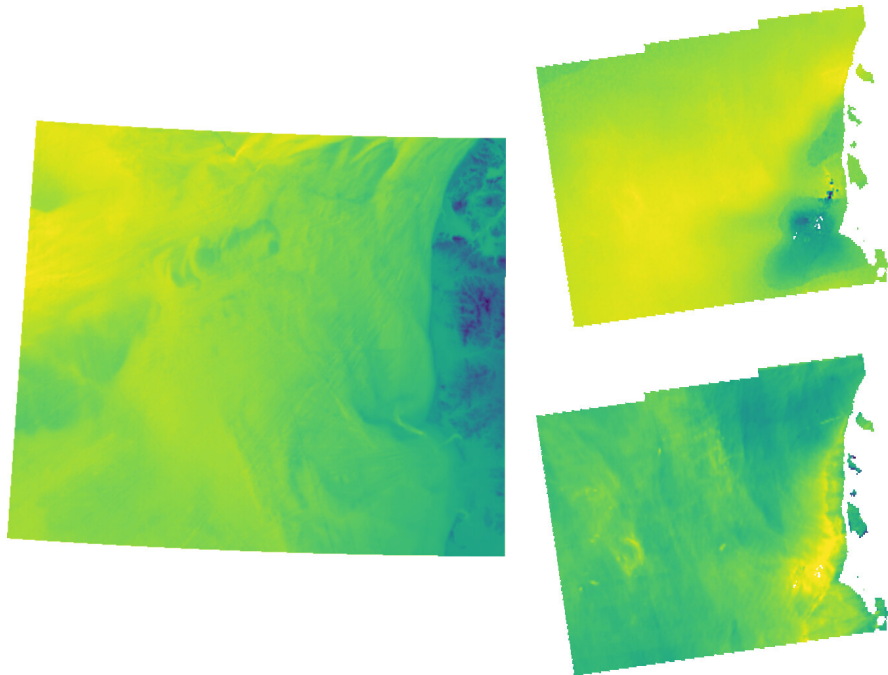


Figure 11: Visualization of ancillary data provided for a fixed area of interest; left: bathymetry, right top: wind direction, and right bottom: wind speed.

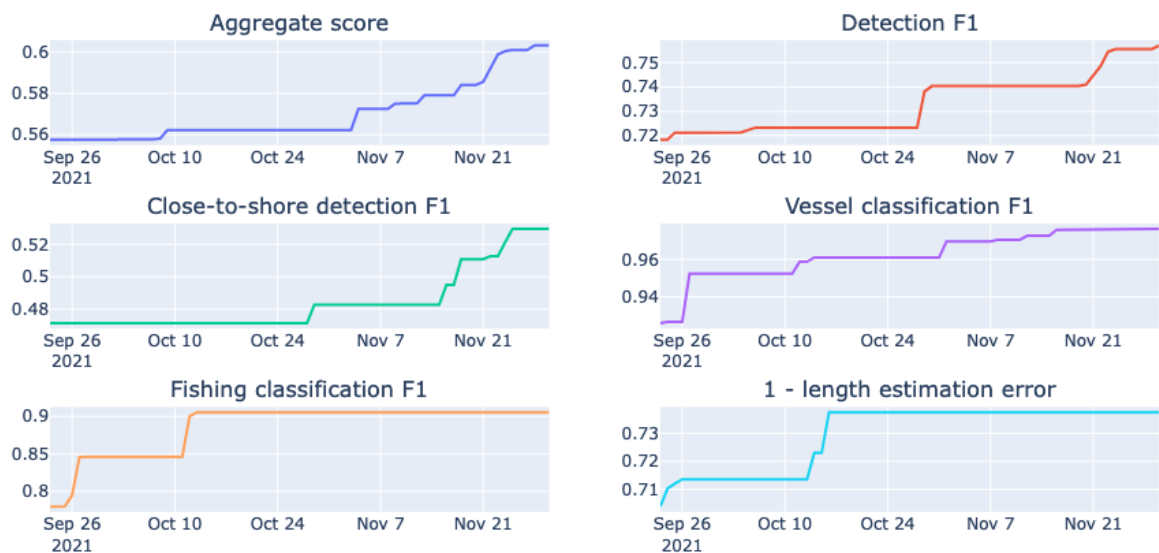


Figure 12: Improvement in aggregate and sub-scores from September–November.

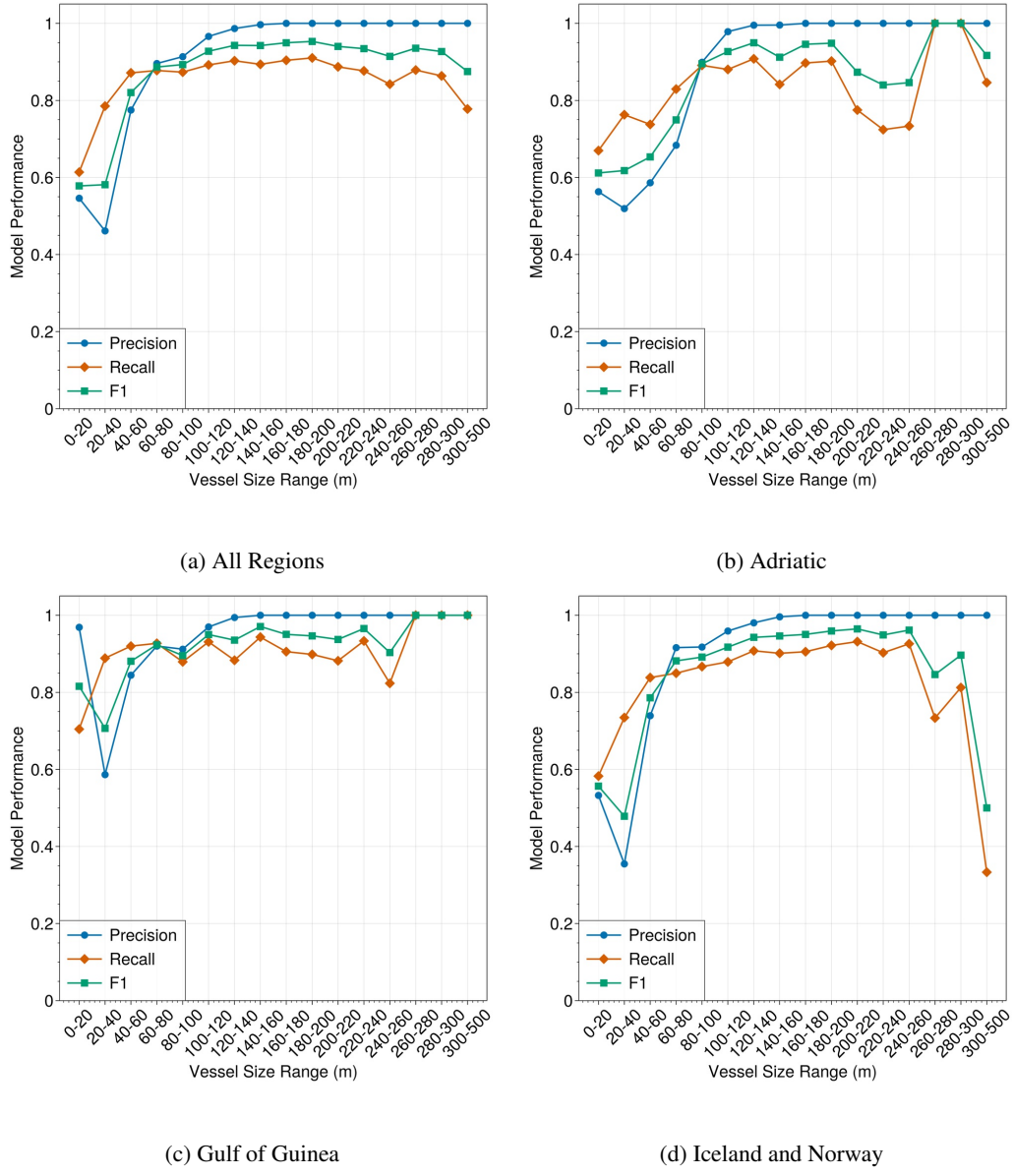


Figure 13: Winning model performance as a function of vessel size on high and medium confidence ground truth data by geographic region.

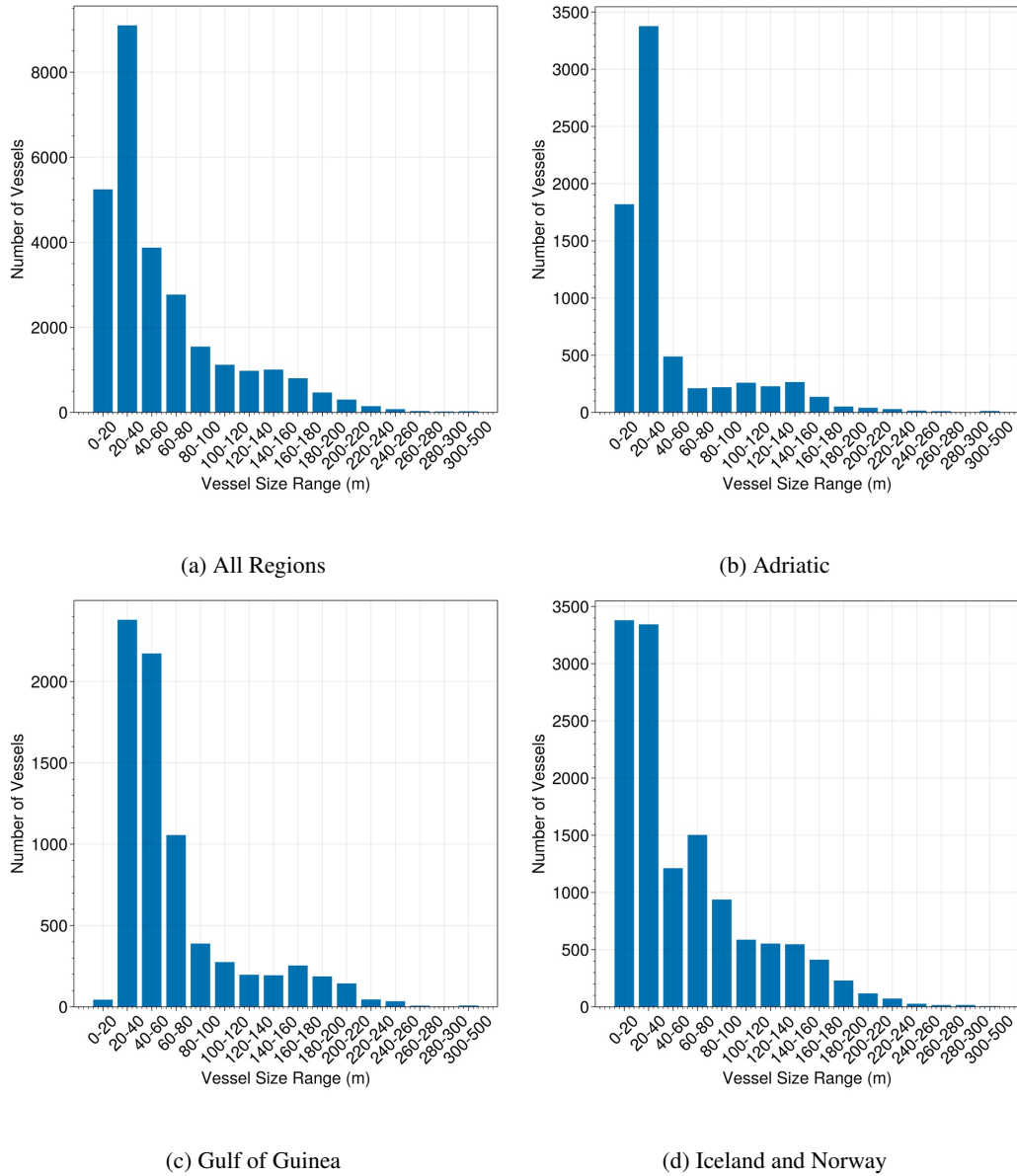


Figure 14: Distribution of vessel size on high and medium confidence ground truth data by geographic region.

F Instructions to expert annotators

In these tasks, you will see a Satellite Synthetic Aperture Radar image. The ground sample distance (GSD) is 20m, meaning that a single pixel is 20 meters over the ground.

The Task is to (1) identify vessels and other vessel-like objects in the imagery and label them as “non-vessels” when one is highly confident that they are not vessels, and label them as “vessels” otherwise; (2) provide a confidence rating.

Contents

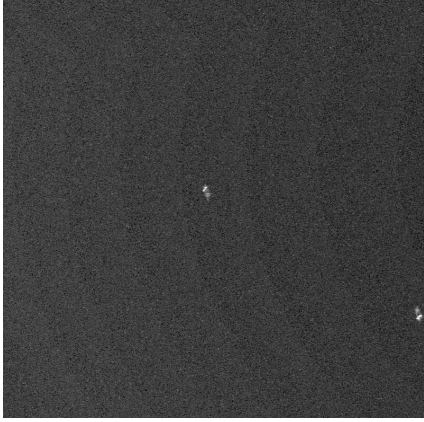
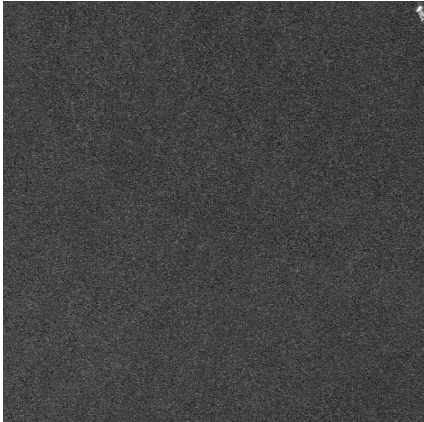
- Labels
- Annotation Rules
- Confidence Rating

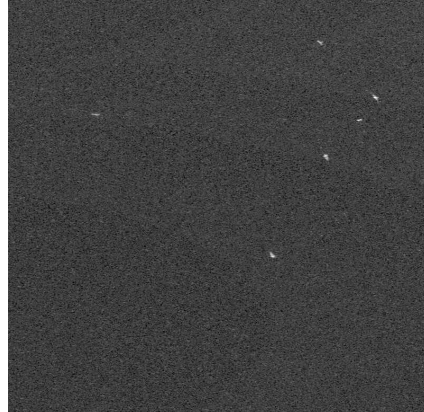
Categories

1. Vessel
2. Non-Vessel

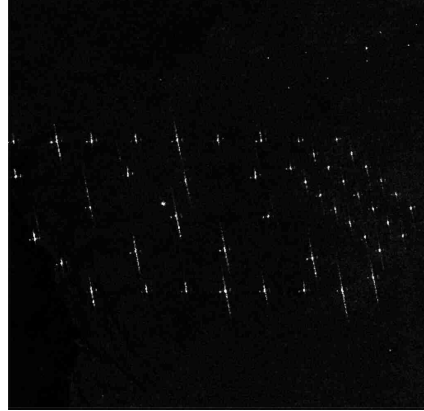
Annotation Rules

Vessels

Description	Example
<p>Example: Place a bounding box around the area of the vessel the box should be tight around the object.</p> <p><i>-In this example there should be two bounding boxes with the annotation for Vessel</i></p>	<p>Vessel example</p> 
<p>Example: In this example there is a single object in the top right of the image chip; annotate with a bounding box.</p> <p><i>-This example would have a single box annotation for vessel</i></p>	<p>Vessel example</p> 

<p>Example: There are six objects in the image; annotate with a bounding box for each object. Note these objects do not form a clear pattern.</p> <p><i>-This example would have six boxes with the annotation vessel</i></p>	<p>Vessel example</p> 
--	---

Non-Vessels

<p>Description</p> <p>Example: This is an example of a wind farm, notable for the orderly pattern and the reflections formed by the objects. Please annotate these objects individually with a bounding box Non-Vessel.</p> <p>Note that vessels may in some instances anchor in grids and they may anchor inside of wind farms. What separates a windmill from a vessel is likely going to be the backscatter from windmill blades.</p>	<p>Example</p> <p>Wind Farm example</p> 
<p>Example: There is a cluster of objects in the center of the image, notable for the orderly pattern and the reflections formed by the objects. The objects in this cluster are windmills. Place a bounding box as Non-Vessel around each object in the cluster.</p> <p>Note that vessels may in some instances anchor in grids and they may anchor inside of wind farms. What separates a windmill from a vessel is likely going to be the backscatter from windmill blades.</p> <p>Note that there are also some objects in the top right hand corner; these are likely vessels. Place a bounding box as Vessel around each object in the top right hand corner.</p>	<p>Non-Vessel and Vessel example</p> 

Negative example

Description	Example
<p>Example: This image is an example of a bridge. The bridge is identifiable as a result of a long narrow line between land masses.</p> <p>Do Not annotate bridges or similar structures.</p> <p>Annotate all other objects that are likely Vessels and Non-Vessels with a bounding box</p>	<p>Negative example</p> 

Confidence Rating

Description: For each annotation, what is your level of confidence for the detection of the object and its vessel/non-vessel label?

Confidence Attribute	Description
High confidence	I am absolutely sure it is a vessel.
Medium confidence	I am not so sure, but it looks like a vessel.
Low confidence	I am mostly guessing it is a vessel.